Electrochemistry

DOI: 10.1002/ange.201301066

An Efficient Three-Dimensional Oxygen Evolution Electrode**

*Jun Wang, Hai-xia Zhong, Yu-ling Qin, and Xin-bo Zhang**

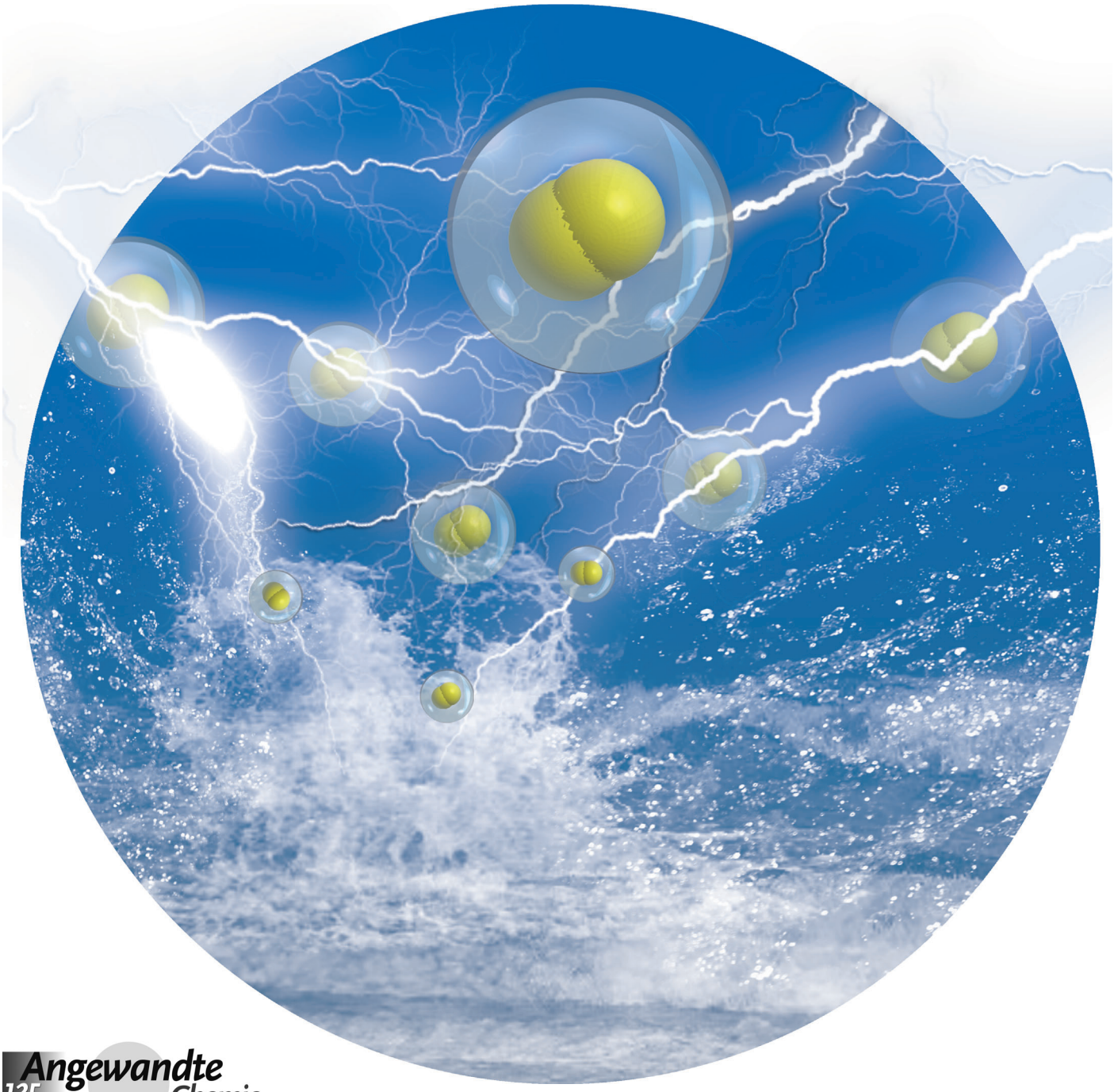

The challenges of meeting the rapidly increasing global energy demand and developing carbon-neutral economy require untiring efforts to exploit and store abundant but diffuse renewable energy sources.[1] Among many innovative approaches, the efficient production of hydrogen serving as fuel, through electricity-driven water splitting, seems promising and appealing.[2] However, the overall efficiency of the reaction is largely impeded by the kinetically sluggish oxygen evolution reaction (OER), imposing serious overpotential requirement.[3] Although precious metal oxides, such as RuO_2 and IrO_2, are considered to be the most active OER electrocatalysts, they are not suitable for large-scale applications because of their scarcity and high costs.[4] In response, non-noble transition-metal-based catalysts, especially nickel (Ni), are becoming focus of growing research interests because of their earth-abundant nature and theoretically high catalytic activity.[5,6] Currently, these non-noble transition-metal-based OER catalysts are usually prepared as thin films from precursor solution containing metal cations by electrodeposition, sputtering, dip-coating, and spin-coating methods on two-dimensional (2D) planar substrates.[5,7] Although significant improvements have been achieved, the activity and stability of the catalyst layer should be further enhanced by optimizing the structural, mechanical, and electrical contact between the catalyst and the substrates.

Compared to the conventional 2D planar architecture, electrodes based on 3D porous materials might improve the activity by increasing the electroactive surface area of the catalysts.[8,9] Taking the advantages of a comparatively high surface area, high electron conductivity, and low costs, Ni foam is generally chosen to serve as template, support, as well as current collector for battery and supercapacitor.[10] However, the Ni foam cannot be directly used as OER electrode because of its intrinsic instability under the OER experimental condition. In response, constructing protective and conductive interlayers, such as porous carbon, to bridge the outermost oxygen evolution catalyst (OEC) layer and the innermost 3D conductive Ni backbone could be a promising strategy. Other than traditional templates such as mesoprous silica and zeolites,[11] zeolite imidazolate framework (ZIF-8) possesses a high carbon content, high chemical and thermal stability, large Brunauer–Emmett–Teller (BET) surface area, and oxygen-free character, making it a novel and promising template for porous carbon synthesis.[12]

To design an efficient OER catalyst with these factors in mind, herein, we first develop a unique approach to fabricate a 3D Ni foam/porous carbon/anodized Ni (NF/PC/AN) electrode, wherein homogeneous coating of the 3D Ni framework with porous carbon membrane plays a key role, which is derived from ZIF-8 and subsequently employed as difunctional interlayer to both protect the inner instable Ni foam and support the outermost Ni OEC layer. It is also the first report that the Ni-based OEC is in situ generated from anodization of the innermost Ni foam skeleton and then penetrated into the voids and finally covered the surface of the porous carbon membrane. Interestingly, the performance of this novel NF/PC/AN electrode is very good for OER, which is considered to be the synergy of the high activity of AN and the high conductivity and stability of the electrode.

Briefly, the facile and scalable fabrication process of the 3D NF/PC/AN electrode (see Scheme S1 in the Supporting Information) is described as follows. The Ni foam is first treated with an acid solution containing polyvinylpyrrolidone (PVP) to remove the possible oxide layer and enhance the affinity of the surface. Then, the Ni foam is immersed in methanolic solution of zinc nitrate and 2-methylimidazole to deposit a ZIF-8 membrane. Next, the as-prepared Ni foam/ZIF-8 is converted to Ni foam/porous carbon under the treatments of calcination in Ar atmosphere and etching the possible Zn species with acid. Finally, anodization is carried out at a constant potential to obtain a 3D NF/PC/AN electrode which can be in situ applied to test the OER activity.

The morphology of ZIF-8 supported on a Ni foam skeleton is characterized by scanning electron microscopy (SEM). As shown in Figure 1 a,b, the surface of the obtained Ni foam/ZIF-8 is quite different from that of a bare Ni foam (Figure S1), revealing the success of depositing a ZIF-8 membrane on a Ni foam. The ZIF-8 membrane is composed of well intergrown polyhedral crystals with sizes of about 0.2 μm. And no obvious defects such as cracks are observed, indicating the continuous formation of the membrane on the homogeneous support of Ni foam. From the cross-sectional view (Figure 1 c), the thickness of the ZIF-8 membrane is measured to be about 4.5 μm. The carbonization of the ZIF-8 membrane is carried out by calcinating the Ni foam/ZIF-8 at 800 °C for 5 h at a heating rate of 3 °C min^{-1} in Ar atmosphere. Although the carbonization temperature is close to the boiling point of Zn and thus may vaporize the carbon-reduced Zn, the obtained sample is also immersed in hydrochloric acid solution (1 M) for 30 minutes to etch the possible Zn species which will poison the OER according to the previous report.[5g] As can be seen in Figure 1 d,e, the morphology of the Ni foam/porous carbon membrane is greatly changed in contrast to Ni foam/ZIF-8, wherein the surface of the carbon membrane has a ladderlike morphology. And the thickness of the carbon membrane is reduced to around 3.5 μm because of the shrink of the ZIF-8 membrane during the carbonization process (Figure 1 f). Notably, from the SEM image of the cross-sectional view, there can be seen many macropores which may result from the evaporation of

[*] J. Wang, H. X. Zhong, Y. L. Qin, Prof. X. B. Zhang
State Key Laboratory of Rare Earth Resource Utilization
Changchun Institute of Applied Chemistry
Chinese Academy of Sciences, Changchun, 130022 (P.R. China)
E-mail: xbzhang@ciac.jl.cn
Homepage: http://energy.ciac.jl.cn
J. Wang, H. X. Zhong, Y. L. Qin
University of Chinese Academy of Sciences
Beijing, 100049 (P.R. China)

[**] This work is financially supported by the 100 Talents Program of the Chinese Academy of Sciences, the National Program on Key Basic Research Project of China (973 program, grant number 2012CB215500), and the National Natural Science Foundation of China (grant numbers 21101147 and 21203176).

Supporting information for this article is available on the WWW under http://dx.doi.org/10.1002/anie.201301066.

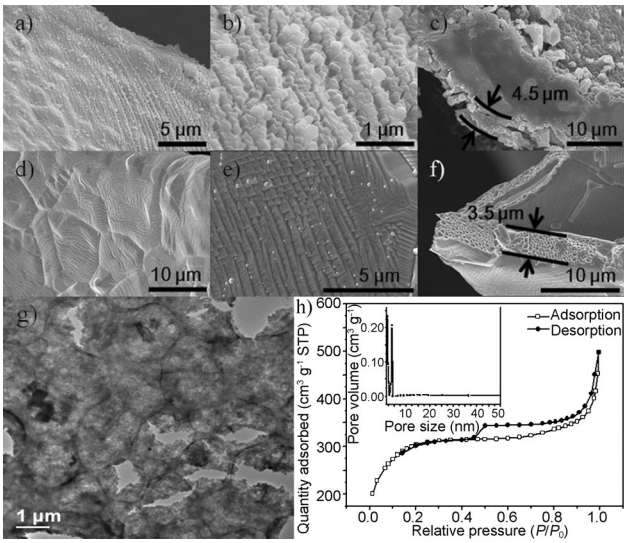

Figure 1. SEM images of a–c) Ni foam/ZIF-8, d–f) Ni foam/porous carbon, and c, f) the according cross-sectional view; g) TEM image of ZIF-8 derived porous carbon membrane obtained by completely etching Ni foam with acid, and h) nitrogen adsorption-desorption isotherm for the obtained porous carbon membrane (inset: pore size distribution; STP = standard temperature and pressure).

carbon-reduced Zn or the subsequent etching of Zn species with acid. Elemental analysis determines that the content of carbon is 0.163 mg cm^{-2}.

To provide details for the carbon membrane, the Ni foam is completely etched. The X-ray diffraction pattern (XRD) profile displays two prominent peaks with 2θ values of 25° and 44° that can be indexed to carbon (002) and (101) diffractions, respectively (Figure S2). No other diffraction peaks are observed, confirming no impurities. Transmission electron microscopy (TEM) reveals that the dense carbon membrane is still well preserved, indicative of its robust character (Figure 1 g). The porous feature of the carbon membrane is further confirmed by N_2 adsorption–desorption measurements (Figure 1 h). The IV-type adsorption–desorption curves show a steep increase at a low relative pressure, suggesting the micropore characteristic, and the hysteresis in the P/P_0 range of 0.4–1.0, indicating the presence of mesopores. The BET surface area and total pore volume are found to be 960 m^2 g^{-1} and 0.62 cm^3 g^{-1}, respectively. From the pore size distribution (Figure 1 h inset), two kinds of pores are observed: micropores (< 2 nm) and mesopores (3–4.5 nm).

The pore-rich structure of the MOF-derived carbon membrane exactly provides voids to penetrate the Ni-based OEC in situ generated from a Ni foam by anodization. The anodization is operated by applying a constant potential of 1 V (vs. Ag/AgCl) in 0.1 M KOH for 2 h. To highlight the advantages of this strategy for electrode design, the Ni foam without covered porous carbon membrane is also treated by the anodization process under identical conditions (Note: the same heat treatment is applied to the Ni foam before use). By comparing the two current density traces of anodization (Figure S3), it is found that the current density of Ni foam/porous carbon shows the gradual rising trend and stabilizes after 2 h at a value of 18.8 mA cm^{-2}. In contrast, the current density of the Ni foam has been declining and reached a final value of 6.8 mA cm^{-2}. After that, the 3D NF/PC/AN electrode and Ni foam electrode are obtained and used for further characterization. Figure 2 a shows the low magnified SEM image of the 3D NF/PC/AN electrode, where the ladderlike morphology of the porous carbon membrane disappears. The high magnified SEM image in Figure 2 b reveals that the surface of the electrode is full of small particles, which will further increase the active sites for OER. Figure 2 c shows the cross-sectional view of the 3D NF/PC/AN electrode. The

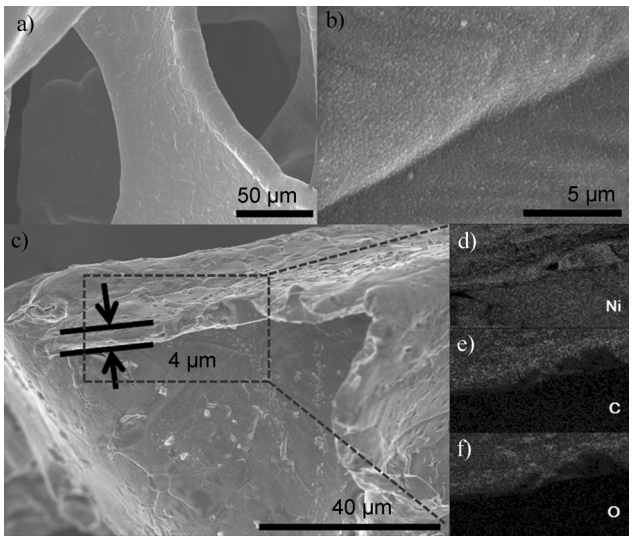

Figure 2. SEM images of the 3D NF/PC/AN electrode obtained by anodization with a) low, b) high magnification, and c) the according cross-sectional view; the element mapping images of d) Ni, e) C, and f) O in the selected area.

thickness of the active layer is measured to be 4 μm, which is a little thicker than a porous carbon membrane, assuming that the Ni-based OEC derived from the Ni foam successfully penetrates through the voids and finally covers the surface of the porous carbon membrane. The element mapping images (Figure 2 d–f) further demonstrate the homogeneous distribution of Ni, C, and O in the active layer, confirming the above assumption. On the contrary, SEM images of the Ni foam electrode (Figure S4) reveal that the resulting dense film has a smooth surface with many cracks that form upon drying and its thickness is even up to 8 μm. From the above observations, we conclude that the porous carbon membrane interlayer on the Ni foam cannot only enhance the mechanical strength of the electrode, preserving the well intact active layer, but also makes possible that the in situ generated Ni-based OEC adheres to the Ni foam substrate, holding the active layer tightly.

Cyclic voltammetry (CV) is directly performed on the in situ obtained 3D NF/PC/AN electrode and the Ni foam electrode to test their OER activities (Figure 3). For the 3D NF/PC/AN electrode, the weak anodic and cathodic waves near 470 and 445 mV (vs. Ag/AgCl) are observed, corre-

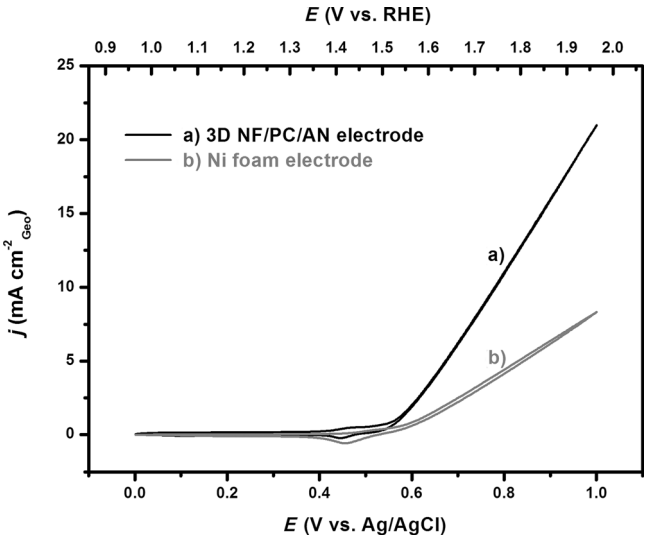

Figure 3. CV scans for a) 3D NF/PC/AN electrode and b) Ni foam electrode in 0.1 M KOH at a sweeping rate of 5 $mV s^{-1}$.

sponding to the $Ni(OH)_2$/NiOOH redox reaction.[5g,13] However, only the Ni foam electrode has a cathodic wave at 455 mV and displays no apparent anodic wave. Both 3D NF/PC/AN electrode and Ni foam electrode reveal the onset potential near 560 mV. When the OER current density reaches 5 $mA cm^{-2}$, the applied potentials need to be 673 mV ($\eta = 407$ mV) for the 3D NF/PC/AN electrode and 830 mV ($\eta = 564$ mV) for the Ni foam electrode. Likewise, when the potential is applied at 800 mV implying $\eta = 534$ mV, the OER current densities of the 3D NF/PC/AN electrode and Ni foam electrode are 10.9 and 4.4 $mA cm^{-2}$, respectively. The performance of AN is even comparable to that of previous noble-metal-based catalysts.[4] As expected, in addition to the above-mentioned adhesive and protective effects, the porous carbon membrane interlayer also behaves like interconnected "highways" for electron transport between the active surface and conductive substrate, leading to a better OER activity of the 3D NF/PC/AN electrode. Compared with the previous reported 2D planar electrode, the 3D NF/PC/AN electrode exerts a superior performance for the OER as well.[5g,13]

To date, there is no consensus on the Ni-based active material that is responsible for the OER. Here, we use ex situ X-ray photoelectron spectroscopy (XPS) and Raman spectroscopy to investigate the 3D NF/PC/AN electrode and Ni foam electrode after anodization. In the Ni 2p region of the XPS spectra (Figure 4a), the 3D NF/PC/AN electrode shows a Ni $2p_{3/2}$ peak at 855.7 eV, and the Ni foam electrode shows a Ni $2p_{3/2}$ peak at 855.4 eV. According to the previous study, the former may originate from $Ni(OH)_2$ or NiOOH, and the latter belongs to NiO.[14] In addition, in the O 1s region (Figure 4b), the 3D NF/PC/AN electrode shows one peak at 531.7 eV, while the Ni foam electrode displays not only a predominant peak at 531 eV, but also a very weak peak at about 529.2 eV. These are also consistent with previous studies on $Ni(OH)_2$, NiOOH, and NiO.[7b,14] In the Raman spectra (Figure 4c), peaks of the 3D NF/PC/AN electrode appear at 479 and 559 cm^{-1}, which match well with γ-NiOOH.[15,16] The Ni foam electrode shows a broad peak range from 400 to 600 cm^{-1}, which may be attributed to the mixture of NiO and $Ni(OH)_2$.[15,17] From the above results, we propose that the Ni foam electrode after anodization is easily dehydrated during the characterization process, which is consistent with its surface morphology (Figure S4). But the 3D NF/PC/AN electrode possesses a better stability, revealing the adhesive and protective effects of the porous carbon membrane again, and facilitates the formation and stabilization of γ-NiOOH which is proved to be a more efficient catalyst for the OER.[5d] Moreover, it should be noted that ZIF-8 containing N-based ligands is regarded to benefit the formation of N-doped carbon which plays a great role in improving the performances of battery, supercapacitor, and oxygen reduction reaction.[18] Here, the porous carbon membrane in the 3D NF/PC/AN electrode is N-doped, which is confirmed by a XPS spectrum (Figure S5). Whether the N-doped porous carbon would give the promotion to the 3D NF/PC/AN electrode for OER requires further work.

The stability tests of the two electrodes are also carried out with continuous CV scans in 0.1 M KOH at a sweeping rate of 5 $mV s^{-1}$. As shown in Figure S6, the 3D NF/PC/AN electrode exhibits a better activity retaining ability than that of the Ni foam electrode after 800 cycles. And the activity degradation of the 3D NF/PC/AN electrode may be ascribed to the increased thickness of the active layer which is still

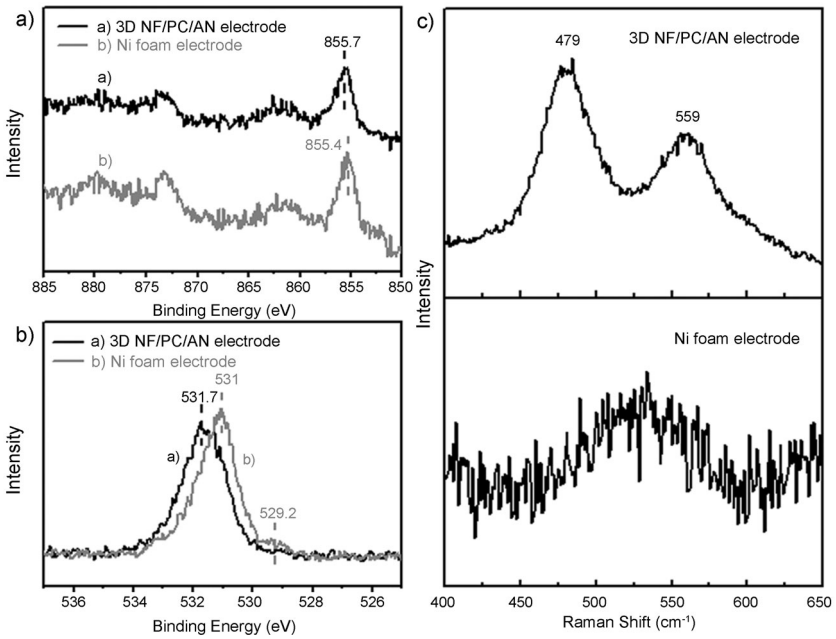

Figure 4. XPS spectra of a) Ni 2p, b) O 1s, and c) Raman spectra for the 3D NF/PC/AN electrode and the Ni foam electrode.

lower than that of the Ni foam electrode before and after cycling (Figure S7), manifesting the protective role of the porous carbon membrane for the Ni foam substrate to suppress excess anodization. Furthermore, inspired by CoPi, CoBi, and NiBi as active catalysts for the OER,[5c–f] the 3D NF/PC/AN electrode and Ni foam electrode are also obtained by anodization at 1 V (vs. Ag/AgCl) in 0.5 M NaPi for 2 h. And the 3D NF/PC/AN electrode also reveals higher OER activity than Ni foam electrode (Figure S8), highlighting the strategy for electrode design.

In summary, we have first successfully prepared a novel 3D NF/PC/AN electrode which combines a 3D Ni foam, serving as the conductive substrate and the source of the in situ generated OEC, with a MOF-derived porous carbon membrane that provides voids to accommodate the OEC, endowing the whole electrode with efficient OER activity and high stability. The significant improvement is attributed to its tailored properties, which are vital to catalytic reactions, including a high activity of AN, an interconnected conductive network, and an enhanced stability of the electrode. We anticipate that the successful design of the OER electrode described here would lead to improved strategies and broaden the scope for future investigations on many other areas, such as lithium-ion batteries, lithium–air batteries, and supercapacitors.

Experimental Section

Preparation of the Ni foam/ZIF-8: The Ni foam (1 cm × 3 cm) was pretreated with 20 mL of HCl solution (1M) containing PVP (0.5 g) to clean its surface and enhance the affinity of the surface. After 30 minutes, the Ni foam was washed with water and methanol to remove excess PVP. Then, the Ni foam was immersed in methanol solution (100 mL) containing $Zn(NO_3)_2$ (50 mM) and 2-methylimidazole (50 mM) without disturbance for about 10 h. The sample was washed with methanol and freeze-dried to obtain Ni foam/ZIF-8.

Preparation of Ni foam/porous carbon: The obtained Ni foam/ZIF-8 was calcinated at 800 °C for 5 h at a heating rate of 3 °C min^{-1} in Ar atmosphere. After that, the sample was immersed in HCl solution (1M) to etch the possible Zn species for 30 minutes. Followed by washing with water and freeze-drying, the Ni foam/porous carbon was obtained.

Preparation of the 3D NF/PC/AN electrode and test OER activity: The electrochemical experiments were measured with a three electrode system at room temperature, wherein Ni foam/porous carbon, Pt plate and Ag/AgCl were used as working electrode, counter electrode, and reference electrode, respectively. The working and counter electrodes were separated by a porous glass frit. To obtain 3D NF/PC/AN electrode, anodization was performed in 0.1M KOH (pH 13) at 1 V (vs. Ag/AgCl) for 2 h. Then CV was directly performed from 0 V to 1 V (vs. Ag/AgCl) at a scanning rate of 5 mV s^{-1} to test OER activity. The anodization and cyclic voltammograms (0–1.5 V vs. Ag/AgCl) were also performed in 0.5 M phosphate buffer solution (pH 7) while the other conditions remained unchanged. The current density was normalized to the geometrical area and the measured potentials versus Ag/AgCl were converted to a reversible hydrogen electrode (RHE) scale according to the Nernst equation ($E_{RHE} = E_{Ag/AgCl} + 0.059\,pH + 0.197$).

Received: February 6, 2013
Published online: April 8, 2013

Keywords: electrochemistry · metal–organic frameworks · oxygen evolution reaction · porous carbon membranes

[1] N. S. Lewis, D. G. Nocera, *Proc. Natl. Acad. Sci. USA* **2006**, *103*, 15729.
[2] a) J. Moorhouse, *Modern Chlor-Alkali Technology*, *Vol. 8*, Wiley-Blackwell, Oxford, **2001**; b) L. M. Gandía, R. Oroz, A. Ursúa, P. Sanchis, P. M. Diéguez, *Energy Fuels* **2007**, *21*, 1699.
[3] a) R. I. Cukier, D. G. Nocera, *Annu. Rev. Phys. Chem.* **1998**, *49*, 337; b) M. H. V. Huynh, T. J. Meyer, *Chem. Rev.* **2007**, *107*, 5004; c) S. Hammes-Schiffer, *Acc. Chem. Res.* **2009**, *42*, 1881.
[4] a) S. Trasatti, *Electrochim. Acta* **1984**, *29*, 1503; b) S. Ardizzone, G. Fregonara, S. Trasatti, *Electrochim. Acta* **1990**, *35*, 263.
[5] a) R. Subbaraman, D. Tripkovic, D. Strmcnik, K. C. Chang, M. Uchimura, A. P. Paulikas, V. Stamenkovic, N. M. Markovic, *Science* **2011**, *334*, 1256; b) R. Subbaraman, D. Tripkovic, K. C. Chang, D. Strmcnik, A. P. Paulikas, P. Hirunsit, M. Chan, J. Greeley, V. Stamenkovic, N. M. Markovic, *Nat. Mater.* **2012**, *11*, 550; c) M. Dincă, Y. Surendranath, D. G. Nocera, *Proc. Natl. Acad. Sci. USA* **2010**, *107*, 10337; d) D. K. Bediako, B. Lassalle-Kaiser, Y. Surendranath, J. Yano, V. K. Yachandra, D. G. Nocera, *J. Am. Chem. Soc.* **2012**, *134*, 6801; e) M. W. Kanan, D. G. Nocera, *Science* **2008**, *321*, 1072; f) Y. Surendranath, M. Dincă, D. G. Nocera, *J. Am. Chem. Soc.* **2009**, *131*, 2615; g) D. A. Corrigan, R. M. Bendert, *J. Electrochem. Soc.* **1989**, *136*, 723.
[6] a) P. W. T. Lu, S. Srinivasan, *J. Electrochem. Soc.* **1978**, *125*, 1416; b) M. Cappadonia, J. Divisek, T. Vonderheyden, U. Stimming, *Electrochim. Acta* **1994**, *39*, 1559.
[7] a) J. Suntivich, K. J. May, H. A. Gasteiger, J. B. Goodenough, Y. Shao-Horn, *Science* **2011**, *334*, 1383; b) L. Trotochaud, J. K. Ranney, K. N. Williams, S. W. Boettcher, *J. Am. Chem. Soc.* **2012**, *134*, 17253; c) T. Hisatomi, H. Dotan, M. Stefik, K. Sivula, A. Rothschild, M. Grätzel, N. Mathews, *Adv. Mater.* **2012**, *24*, 2699.
[8] a) C. Zhu, Y. Yu, L. Gu, K. Weichert, J. Maier, *Angew. Chem.* **2011**, *123*, 6402; *Angew. Chem. Int. Ed.* **2011**, *50*, 6278; b) J. Guo, Y. Xu, C. Wang, *Nano Lett.* **2011**, *11*, 4288; c) J. Jiang, Y. Li, J. Liu, X. Huang, C. Yuan, X. W. Lou, *Adv. Mater.* **2012**, *24*, 5166; d) S. Xin, Y. G. Guo, L. J. Wan, *Acc. Chem. Res.* **2012**, *45*, 1759; e) Y. P. Zhai, Y. Q. Dou, D. Y. Zhao, P. F. Fulvio, R. T. Mayes, S. Dai, *Adv. Mater.* **2011**, *23*, 4828.
[9] a) H. Zhang, X. Yu, P. V. Braun, *Nat. Nanotechnol.* **2011**, *6*, 277; b) X. Lang, A. Hirata, T. Fujita, M. Chen, *Nat. Nanotechnol.* **2011**, *6*, 232; c) J. Kibsgaard, Y. Gorlin, Z. Chen, T. F. Jaramillo, *J. Am. Chem. Soc.* **2012**, *134*, 7758.
[10] a) Z. Chen, W. Ren, L. Gao, B. Liu, S. Pei, H. M. Cheng, *Nat. Mater.* **2011**, *10*, 424; b) Y. H. Chang, C. T. Lin, T. Y. Chen, C. L. Hsu, Y. H. Lee, W. Zhang, K. H. Wei, L. J. Li, *Adv. Mater.* **2012**, DOI: 10.1002/adma.201202920; c) C. Yuan, J. Li, L. Hou, X. Zhang, L. Shen, X. W. Lou, *Adv. Funct. Mater.* **2012**, *22*, 4592.
[11] a) Y. Fang, D. Gu, Y. Zou, Z. Wu, F. Li, R. Che, Y. Deng, B. Tu, D. Zhao, *Angew. Chem.* **2010**, *122*, 8159; *Angew. Chem. Int. Ed.* **2010**, *49*, 7987; b) C. G. Wu, T. Bein, *Science* **1994**, *266*, 1013; c) S. H. Joo, S. J. Choi, I. Oh, J. Kwak, Z. Liu, O. Terasaki, R. Ryoo, *Nature* **2001**, *412*, 169.
[12] a) H. L. Jiang, B. Liu, Y. Q. Lan, K. Kuratani, T. Akita, H. Shioyama, F. Zong, Q. Xu, *J. Am. Chem. Soc.* **2011**, *133*, 11854; b) W. Chaikittisilp, M. Hu, H. Wang, H. S. Huang, T. Fujita, K. C. W. Wu, L. C. Chen, Y. Yamauchi, K. Ariga, *Chem. Commun.* **2012**, *48*, 7259.
[13] D. A. Corrigan, *J. Electrochem. Soc.* **1987**, *134*, 377.
[14] a) M. C. Biesinger, B. P. Payne, L. W. M. Lau, A. Gerson, R. S. C. Smart, *Surf. Interface Anal.* **2009**, *41*, 324; b) E. L. Ratcliff, J. Meyer, K. X. Steirer, A. Garcia, J. J. Berry, D. S. Ginley, D. C. Olson, A. Kahn, N. R. Armstrong, *Chem. Mater.* **2011**, *23*, 4988.
[15] B. S. Yeo, A. T. Bell, *J. Phys. Chem. C* **2012**, *116*, 8394.

[16] J. Desilvestro, D. A. Corrigan, M. J. Weaver, *J. Phys. Chem.* **1986**, *90*, 6408.
[17] a) R. Kostecki, F. McLarnon, *J. Electrochem. Soc.* **1997**, *144*, 485; b) J. Landon, E. Demeter, N. I?nog?lu, C. Keturakis, I. E. Wachs, R. Vasic, A. I. Frenkel, J. R. Kitchin, *ACS Catal.* **2012**, *2*, 1793.
[18] a) Y. Zhao, C. Hu, Y. Hu, H. Cheng, G. Shi, L. Qu, *Angew. Chem.* **2012**, *124*, 11533; *Angew. Chem. Int. Ed.* **2012**, *51*, 11371; b) Y. Zheng, Y. Jiao, J. Chen, J. Liu, J. Liang, A. J. Du, W. M. Zhang, Z. H. Zhu, S. C. Smith, M. Jaroniec, G. Q. Lu, S. Z. Qiao, *J. Am. Chem. Soc.* **2011**, *133*, 20116; c) Z. S. Wu, W. Ren, L. Xu, F. Li, H. M. Cheng, *ACS Nano* **2011**, *5*, 5463.

